On the Buckling of Stiffened Imperfect Cylindrical Shells

J. Arbocz* and E.E. Sechler†
California Institute of Technology, Pasadena, Calif.

A theoretical investigation of the buckling behavior of imperfect ring and stringer stiffened shells under axial compression was carried out. The nonlinear Donnell-type equations for imperfect shells with "smeared out" ring and stringer stiffeners have been reduced to an equivalent set of nonlinear ordinary differential equations. The resulting two-point boundary value problem was solved numerically by the "shooting method." The use of this method made it possible to investigate how the axial load level at the limit point is affected by the following factors: the prebuckling growth caused by the edge constraint, different sets of boundary conditions, the orientation and shape of the axisymmetric and asymmetric imperfection components and the eccentricity in the load application. As a result of this investigation, a simple formula is proposed which makes it possible to take into account both the effect of initial imperfections and the effect of the appropriate boundary conditions.

Nomenclature

A_0, A_1 = axial dependence of the radial imperfection Eq. (5)
c = Poisson's effect ($c=\sqrt{3(1-\nu^2)}$)
$C_1 \ldots C_{29}$ = coefficients in Eqs. (14-17)[13]
D_{xx}, D_{xy}, D_{yy} = effective bending stiffnesses[9]
E = Young's modulus (lb/in^2)
f = vector function, Eq. (19)
F, f_0, f_1, f_2 = Airy stress functions, Eq. (7)
H_{xx}, H_{xy}, H_{yy} = effective stretching stiffnesses,[9]
L = shell length
L_D, L_H, L_Q = linear operators defined by Eq. (3)
L_{NL} = nonlinear operator defined by Eq. (4)
M_x = moment resultant (in-lb/in.)
n = number of full waves in the circumferential direction
N_x, N_{xy} = stress resultants (lb/in.)
N_{xM} = perfect shell buckling load, see Table 2 (lb/in.)
P = nondimensional potential energy of the system
q = load eccentricity measured from the skin midsurface, positive inward
$\bar{q}$ = nondimensional load eccentricity ($=4cRq/t^2$)
Q_x = transverse shear resultant (lb/in.)
Q_{xx}, Q_{xy}, Q_{yy} = effective torsional stiffnesses[9]
R = radius of shell
S, T = dummy arguments used in Eq. (4)
u, v = in-plane displacement components
U = potential energy of the system (in-lb)
$\bar{W}$ = radial imperfection from perfect circular cylinder
W, w_0, w_1 = radial displacement, positive inward, Eq. (6)
W_ν = Poisson's expansion ($=-\nu c\bar{H}_{xx}\lambda/(1+\mu_1)$)
x, y = axial and circumferential coordinates on the middle surface of the shell, respectively
$\bar{x}, \bar{y}$ = nondimensional coordinates ($\bar{x}=x/R, \bar{y}=y/R$)
Y = unified vector variable, Eq. (19)
α_2 = ring stiffener parameter[9]
δ = end shortening
ϵ_x = strain component
μ_2, χ_1, χ_2 = stiffener parameters[9]
λ = nondimensional loading parameter ($=c\sigma R/Et$)
ν = Poisson's ratio
ρ = nondimensional loading parameter ($=N_x/N_{x_M}$)
σ = applied compressive stress (lb/in.^{2})

Received Jan. 19, 1976; revision received April 14, 1976. The authors are indebted to C.D. Babcock, Jr. for many helpful suggestions and for fruitful discussions. The major support of this work was by NSF through Grant GK 16934, although most of the computer runs were done during the first author's tenure at the DFVLR-Forschungszentrum Braunschweig as a "Senior U.S. Scientist Awardee" of the von Humboldt foundation. Both of these aids are gratefully acknowledged.

Index category: Structural Stability Analysis.

*Senior Research Fellow in Aeronautics; presently Professor of Aircraft Structures, Delft University of Technology, The Netherlands. Member AIAA.

†Professor of Aeronautics. Fellow AIAA.

Introduction

PRATICALLY all modern aerospace vehicles are composed of stiffened or unstiffened shells, since these thin-walled structures exhibit very favorable strength over weight ratios. Unfortunately, they are also very prone to buckling instabilities. Thus it is not surprising that, since the beginning of the space age, literally hundreds of technical papers dealing with shell stability have been published. For a comprehensive review of the state-of-the-art of shell design, the reader is referred to the Proceedings of the Thin Shell Structures Symposium, held in 1972 at the California Institute of Technology, edited by Fung and Sechler.[1]

By adding ring and stringer stiffeners the load-carrying capability of isotropic shells can be substantially increased with little weight penalty. Recent analytical[2,3] and experimental[4] studies have shown that, in addition to initial geometric imperfections, the load-carrying capacity of stiffened shell structures can be greatly influenced by a variety of support conditions, by the nonlinear prebuckling deformation caused by the edge constraints and by the location of the load application point.

When investigating the effect of initial imperfections, it has been standard practice to neglect the previous factors[3,5,6,7] in order to simplify the mathematical problem that must be solved. However, in a recent work Arbocz and Sechler[8] presented a solution for the case of axially compressed isotropic shells with both axisymmetric and asymmetric imperfections, where a rigorous satisfaction of the experimental boundary conditions was included.

In this paper this method is extended to include ring-and-stringer-stiffened shells. The purpose of this "extended analysis" was to provide justification for the aforementioned simplified analyses by obtaining solutions that would include the effect of prebuckling deformations due to the edge constraints and would satisfy rigorously the experimental boundary conditions. In addition, it is shown that, by introducing the concept of "end shortening", it is possible to integrate around the limit point of the nonlinear prebuckling equilibrium states without encountering the usual convergence difficulties at axial load levels close to the limit point.

Theoretical Analysis

Assuming the radial displacement W is positive inward and the membrane stress resultants can be obtained from an Airy stress function F as $N_x = F_{,yy}, N_y = F_{,xx}$ and $-F_{,xy}$, then the Donnell-type equations for imperfect stiffened cylindrical shells can be written as

$$L_H(F) - L_Q(W) = -1/R W_{,xx} - 1/2 L_{NL}(W, W+2\overline{W}) \quad (1)$$

$$L_Q(F) + L_D(W) = 1/R F_{,xx} + L_{NL}(F, W+\overline{W}) \quad (2)$$

where the linear operators are

$$\begin{aligned} L_H(\,) &= H_{xx}(\,)_{,xxxx} + H_{xy}(\,)_{,xxyy} + H_{yy}(\,)_{,yyyy} \\ L_Q(\,) &= Q_{xx}(\,)_{,xxxx} + Q_{xy}(\,)_{,xxyy} + Q_{yy}(\,)_{,yyyy} \\ L_D(\,) &= D_{xx}(\,)_{,xxxx} + D_{xy}(\,)_{,xxyy} + D_{yy}(\,)_{,yyyy} \end{aligned} \quad (3)$$

and the nonlinear operator is

$$L_{NL}(S,T) = S_{,xx}T_{,yy} - 2S_{,xy}T_{,xy} + S_{,yy}T_{,xx} \quad (4)$$

Commas in the subscripts denote repeated partial differentiation with respect to the independent variables following the comma. The stiffener properties have been "smeared out" to arrive at effective bending, stretching and torsional stiffnesses for the skin-stiffener combination. The stiffener parameters $D_{xx}, H_{xx}, Q_{xx}, D_{xy}, \ldots$.etc. are defined in Ref. 9. These equations were first derived by Geier,[10] however, in the present notation they are due to Singer[11] and Hutchinson and Amazigo.[3] The cylinder geometry and the coordinate system used is shown in Fig. 1.

For the case of no stiffeners, Eqs. (1) and (2) reduce to the well-known governing equations for an isotropic imperfect cylindrical shell.[12] Thus Eqs. (1) and (2) govern the case of an isotropic shell as well as the case of a shell with any combination of closely-spaced ring and/or stringer stiffeners.

Reduction to an Equivalent Set of Ordinary Differential Equations

If we assume that the initial imperfection surface can be represented as

$$\overline{W}(\bar{x},\bar{y}) = t A_0(\bar{x}) + t A_1(\bar{x}) \cos n\bar{y} \quad (5)$$

where $A_0(\bar{x})$ and $A_1(\bar{x})$ are known functions of $\bar{x}$, then Eqs. (1) and (2) admit separable solutions of the form

$$W(\bar{x},\bar{y}) = tW_v + tw_0(\bar{x}) + tw_1(\bar{x}) \cos n\bar{y} \quad (6)$$

$$\begin{aligned} F(\bar{x},\bar{y}) = ERt^2/c\{ &-1/2\lambda\bar{y}^{-2} + f_0(\bar{x}) \\ &+ f_1(\bar{x}) \cos n\bar{y} + f_2(\bar{x}) \cos 2n\bar{y}\} \end{aligned} \quad (7)$$

Assuming the axial dependence of the response to be an unknown function of $\bar{x}$ will reduce the buckling problem to the solution of a set of nonlinear ordinary differential equations, which will allow the rigorous enforcing of the experimental boundary conditions. The value of the Poisson's expansion $W_v (= -\nu/c\ H_{xx}\lambda/1+\mu_1))$ is obtained by enforcing the circumferential periodicity condition.[13]

Substituting the expressions for $\overline{W}$, W and F into the compatibility Eq. (1), using some trigonometric identities, and finally equating coefficients of like terms, results in the following system of three nonlinear ordinary differential equations

$$\begin{aligned} &\overline{H}_{xx} f_0^{iv} - t/2R\overline{Q}_{xx} w_0^{iv} + cw_0'' - ct/4Rn^2 [w_1''(w_1+2A_1) \\ &\quad + 2w_1'(w_1'+2A_1') + w_1(w_1''+2A_1'')] = 0 \end{aligned} \quad (8)$$

$$\begin{aligned} &\overline{H}_{xx} f_1^{iv} - n^2\overline{H}_{xy} f_1'' + n^4\overline{H}_{yy} f_1 - t/2R(\overline{Q}_{xx} w_1^{iv} \\ &\quad - n^2\overline{Q}_{xy} w_1'' + n^4\overline{Q}_{yy} w_1) \\ &\quad + cw_1'' - ct/2Rn^2 [w_0''(w_1+2A_1) \\ &\quad + w_1(w_0''+2A_0'')] = 0 \end{aligned} \quad (9)$$

$$\begin{aligned} &\overline{H}_{xx} f_2^{iv} - 4n^2\overline{H}_{xy} f_2'' + 16n^4\overline{H}_{yy} f_2 - ct/4Rn^2 [w_1''(w_1+2A_1) \\ &\quad - 2w_1'(w_1'+2A_1') + w_1(w_1''+2A_1'')] = 0 \end{aligned} \quad (10)$$

Substituting in turn the expressions assumed for $\overline{W}, W$ and F into the equilibrium Eq. (2) and applying Galerkin's procedure yields the following system of two nonlinear ordinary differential equations

$$\begin{aligned} &2\overline{Q}_{xx} f_0^{iv} + t/R\overline{D}_{xx} w_0^{iv} - 4cR/t f_0'' + 4c\lambda(w_0''+A_0'') \\ &\quad + 2cn^2 [(w_1+A_1) f_1'' + 2(w_1'+A_1') f_1' \\ &\quad + (w_1''+A_1'') f_1] + 4c\lambda(w_0''A_0'') = 0 \end{aligned} \quad (11)$$

$$\begin{aligned} &2(\overline{Q}_{xx} f_1^{iv} - n^2\overline{Q}_{xy} f_1'' + n^4\overline{Q}_{yy} f_1) + t/R(\overline{D}_{xx} w_1^{iv} - n^2\overline{D}_{xy} w_1'' \\ &\quad + n^4\overline{D}_{yy} w_1) - 4cR/t f_1'' + 4c\lambda(w_1''+A_1'') \\ &\quad + 2cn^2 [2(w_1+A_1) f_0'' \\ &\quad + 2(w_0''+A_0'') f_1 + (w_1+A_1) f_2'' + 4(w_1'+A_1') f_2' \\ &\quad + 4(w_1''+A_1'') f_2] = 0 \end{aligned} \quad (12)$$

The nondimensional stiffener parameters $\overline{D}_{xx}, \overline{H}_{xx}, \overline{Q}_{xx}, \ldots$ are listed in Ref. 9 and $' = d/d\bar{x}$.

Equation (8) can be integrated twice to yield

$$\overline{H}_{xx} f_0'' - t/2R\overline{Q}_{xx} w_0'' + cw_0 - ct/4Rn^2 (w_1+2A_1) w_1 = 0 \quad (13)$$

where the constants of integration are set equal to zero in order to satisfy periodicity.[13] With the help of Eqs. (8) and (13) we can then eliminate the terms f_1^{iv} abd f_0'' from Eqs. (11) and (12). To be able to use the "shooting method" of Ref. 8, it is further necessary to eliminate the w_1^{iv} term from Eq. (9) and the f_1^{iv} term from Eq. (12). This can be accomplished with the help of Eqs. (12) and (9) respectively. Finally some further regrouping makes it possible to write the resulting equations as

$$\begin{aligned} f_1^{iv} &= C_1 f_1'' - C_2 f_1 - C_3 w_1'' - C_4\lambda(w_1''+A_1'') + C_5 w_1 \\ &\quad + C_6 [w_0''(w_1+2A_1) + w_1(w_0''+2A_0'')] - C_7(w_1+A_1) w_0'' \\ &\quad + C_8(w_1+A_1) w_0 - C_9(w_1+A_1)(w_1+2A_1) w_1 \\ &\quad - C_{10} [2(w_0''+A_0'') f_1 + (w_1+A_1) f_2'' + 4(w_1'+A_1') f_2 \\ &\quad + 4(w_1''+A_1'') f_2] \end{aligned} \quad (14)$$

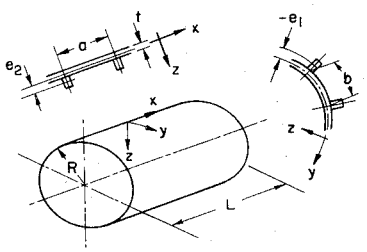

Fig. 1 Cylinder geometry and coordinate axes.

$$f_2^{iv} = C_{11}f_2'' - C_{12}f_2 + C_{13}[w_1''(w_1+2A_1) - 2w_1'(w_1'+2A_1') + w_1(w_1''+2A_1'')] \quad (15)$$

$$w_1^{iv} = C_{14}w_0'' - C_{15}w_0 - C_{16}[w_1''(w_1+2A_1) + 2w_1'(w_1'+2A_1') + w_1(w_1''+2A_1'')] + C_{17}(w_1+2A_1)w_1 - C_{18}[(w_1+A_1)f_1'' + 2(w_1'+A_1')f_1' + (w_1''+A_1'')f_1] - C_{19}\lambda(w_0''+A_0'') \quad (16)$$

$$w_1^{iv} = C_{20}w_1'' - C_{21}w_1 + C_{22}f_1'' - C_{23}\lambda(w_1''+A_1'') - C_{24}f_1 - C_{25}[w_0''(w_1+2A_1) + w_1(w_0''+2A_0'')] - C_{26}(w_1+A_1)w_0'' + C_{27}(w_1+A_1)w_0 - C_{28}(w_1+A_1)(w_1+2A_1)w_1 - C_{29}[2(w_0''+A_0'')f_1 + (w_1+A_1)f_2'' + 4(w_1'+A_1')f_2' + 4(w_1''+A_1'')f_2)] \quad (17)$$

The constants $C_1 - C_{29}$ are listed in Ref. 13. The C-3 boundary conditions ($W = W_{,x} = v = 0$; $N_x = \sigma t$) expressed in terms of the assumed unknown functions become

$$w_0 = -W_v \qquad \text{at } \bar{x} = 0, L/R$$

$$w_1 = w_0' = w_1' = f_1 = f_2 = f_1'' = f_2'' = 0 \quad (18)$$

A list of the reduced boundary conditions and details of the derivation can be found in Ref. 13.

Introducing, as a unified variable, the 16-dimensional vector Y defined as follows

$$Y_1 = f_1,\ Y_2 = f_2,\ Y_3 = w_0,\ Y_4 = w_1,\ Y_5 = f_1', \ldots, Y_{16} = w_1'''$$

then the system of Eqs. (14-18) can be reduced to the following nonlinear 2-point boundary value problem (using the C-3 boundary condition)

$$\frac{d}{d\bar{x}}Y = f(\bar{x}, Y; \lambda) \qquad \text{for } 0 \le \bar{x} \le L/R$$

$$Y_3 = -W_v \qquad \text{at } \bar{x} = 0, L/R \quad (19)$$

$$Y_1 = Y_2 = Y_4 = Y_7 = Y_8 = Y_9 = Y_{10} = 0$$

The solution of this nonlinear 2-point boundary value problem will then locate the limit point of the prebuckling states. By definition the value of the loading parameter λ corresponding to the limit point can be obtained by plotting the maximum amplitude of the asymmetric component of the prebuckling deformation vs axial load level (Fig. 2). Using load increments the solution fails to converge beyond the limit point. This situation is somewhat unsatisfactory, especially since, without the appropriate starting values, the nonlinear iteration scheme will fail to converge also at axial load levels less than the theoretical buckling load. A closer look at the solution curve presented in Fig. 2 reveals, however, that one

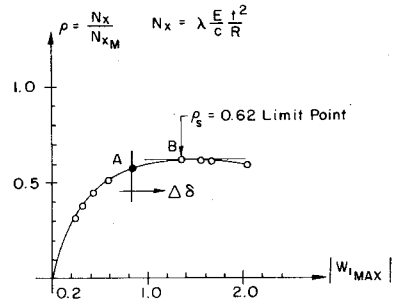

Fig. 2 Load vs asymmetric response for shell XS-1 (SS-3 boundary condition- $N_x = v = W = M_x = 0$).

should be able to extend the response curve beyond the limit point by using increments in deformation instead of increments in loading.

Following Ref. 14, let us define "unit end shortening" as

$$\epsilon = -\frac{1}{2\pi RL}\int_0^{2\pi R}\int_0^L (u_{,x} - qW_{,xx})\,dxdy \quad (20)$$

where

$$u_{,x} = \epsilon_x - 1/2W_{,x}(W_{,x} + 2\overline{W}_{,x}) \quad (21)$$

$$\epsilon_x = 1/\alpha_2(1-\nu^2)/Et[F_{,yy} - \nu F_{,xx}/(1+\mu_2)] + \chi_1/\alpha_2 W_{,xx} - 1/\alpha_2\nu\chi_2/(1+\mu_2)W_{,yy} \quad (22)$$

Introducing these expressions into Eq. (20), substituting for W, $\overline{W}$ and F from Eqs. (5 – 7), carrying out the y-integration, substituting for f_0'' from Eq. (13), introducing $\epsilon_{cl} = t/cR$ and the usual nondimensional parameters, yields

$$\delta = \epsilon/\epsilon_{cl} = \overline{H}_{yy}\lambda + t/2L\{\overline{Q}_{xx}[\nu/(1+\mu_2)\overline{H}_{yy}/\overline{H}_{xx} - (1+\mu_2)/\nu] + t\overline{q}/2R\}\int_0^{L/R} w_0''d\bar{x} - \nu/(1+\mu_2)\overline{H}_{yy}/\overline{H}_{xx}cR/L\int_0^{L/R}[w_0 - n^2t/4R(w_1+2A_1)w_1]d\bar{x} + ct/2L\int_0^{L/R}[w_0'(w_0'+2A_0') + 1/2\,w_1'(w_1'+2A_1')]d\bar{x}^0 \quad (23)$$

where the terms involving the integrals represent the nonlinear part of the end-shortening. When the solution of the boundary value problem (19) has converged, it is advantageous to solve for δ_{NL} by solving the associated initial value problems, rather than using numerical integration schemes. Here we must solve

$$d/d\bar{x}\delta_{NL} = t/2L\{\overline{Q}_{xx}[\nu/(1+\mu_2)\overline{H}_{yy}/\overline{H}_{xx} - (1+\mu_2)/\nu] + t/2R\overline{q}\}w_0'' - \nu(1+\mu_2)\overline{H}_{yy}/\overline{H}_{xx} cR/L[w_0 - n^2t/4R(w_1+2A_1)w_1] + ct/2L[w_0'(w_0'+2A_0') + 1/2w_1'(w_1'+2A_1')]$$

$$\delta_{NL}(0) = 0$$

$$\delta_{NL}(L/R) = \delta_0 \quad (24)$$

This initial value problem, expressed in terms of the unified vector variable Y, represents the one additional equation needed when solving the 2-point boundary value problem (Eq. 19) using increments in "end shortening" instead of increments of axial loading.[15]

Numerical Analysis

Due to the highly nonlinear nature of the above 2-point boundary value problem, anything but a numerical solution is out of the question. All the known numerical techniques for the solution of nonlinear equations involve iterative improvements of initial guesses of the solution. Working with isotropic shells it was found[8] that it is more efficient to adjust the initial guesses of the solution at a limited number of "matching points" rather than trying to adjust the solution at all points along the interval simultaneously, as is required by the standard finite difference schemes. A detailed description of this method, known as "Parallel Shooting" is given in Ref. 8 when using increments in axial load $\Delta\lambda$ and in Ref. 15 when using increments in end-shortening $\Delta\delta_{NL}$. This method is slower than a coarse standard finite difference or finite-element scheme; however, if the length of the intervals of integration is chosen properly so that numerical instabilities are avoided, then this method gives more accurate results. Also since the step size is changed automatically so as to satisfy the chosen convergence criterion, it is unnecessary to repeat the solution with different step sizes to ascertain that a properly converged solution has been found, as is the recommended engineering practice with the standard finite difference or finite-element codes.

The solution was started at a sufficiently low axial load level $\lambda(=c\sigma R/Et)$, so that values from the linearized solution could be used as starting values for the nonlinear iteration scheme. Solutions of the linearized problem were also obtained by the "shooting method."[16] It is well known that, for the linearized 2-point boundary value problem, Newton's method yields the correct initial value S directly without the need of iterations.[17] The solution of the associated initial value problems and the variational equations was done by the library subroutine DEQ from Caltech's Willis Booth Computer Center. DEQ uses the method of Runge-Kutta-Gill to compute starting values for an Adams-Moulton corrector-predictor scheme. The program includes an option with variable interval size and uses automatic truncation error control. For the shells with an $L/R=1.0$ parallel shooting over 8 intervals was used. This actually involved the numerical integration of six 272 dimensional vector equations and of two 144 dimensional vector equations. These high dimensions were due to the simultaneous integration of the variational equations and the corresponding associated initial value problem. It took about 25 sec on the IBM 370/158 to complete one iteration. For proper convergence (5 digits accuracy) at low axial load levels 2 iterations were sufficient; however, at load levels close to the limit point 6-12 iterations would be needed to obtain the same level of convergence. Thus, upon reaching a load level corresponding to point A in Fig. 2, instead of further increments in the axial load $\Delta\lambda$, increments in the nonlinear part of the end-shortening $\Delta\delta$ were used to continue the integration. As can be seen from Figs. 2 and 3, this switch in increments made it possible to integrate around the limit point at B and get converged solutions on the decreasing portions of the solution curve. Also by switching to increments in end-shortening $\Delta\delta$ one avoided the need for taking many very small axial load increments $\Delta\lambda$, which otherwise would be necessary in order to define accurately the location of the limit point B. This resulted in considerable savings in computer time.

Numerical Results

As mentioned earlier, the experimental boundary conditions have a pronounced effect on the buckling load of stringer stiffened shells.[18] To investigate these effects in the presence of initial imperfections the buckling loads of the stringer stiffened shell XS-1 for 4 different sets of boundary conditions were calculated. The shell dimensions and the stiffener parameters are summarized in Table 1. The imperfection modes included in the analysis are shown on the respective figures. To be able to properly assess the effect of the initial imperfections, it is necessary first to calculate the buckling loads of the corresponding perfect shells.

Table 1 Geometric and material properties of shell XS-1

t	0.00774
L	4.0
b	0.316
R/t	517
L/R	1.0
A/bt	0.506
I/bt^3	0.2466
$-e/t$	1.71
E(psi)	10.10^6
Number of stiffeners	80

All dimensions in inches unless otherwise indicated. $v=0.3$.

Buckling Loads of the Perfect Shells

The buckling loads of the perfect shells for the 4 different sets of boundary conditions were calculated by the SRA[19] computer code. This code was selected because it employs a numerical integration scheme similar to the one used by the extended analysis for the imperfect shell buckling load calculations. Thus convergence is controlled by the "error bound" specified and the program selects the step sizes internally to satisfy it. This eliminates the need for repeated runs with different step sizes to verify convergence, as is the recommended engineering practice with standard finite difference or finite-element codes.

In the SRA computer code one can use either a linear or a nonlinear prebuckling solution and then calculate the axial load level at which bifurcation into an asymmetric pattern will occur. It is the user's responsibility to select the range of circumferential wave numbers for which the search of the lowest bifuraction load is to be carried out. Since a plot of bifurcation load vs circumferential wave number contains several local minimums, it requires some engineering insight to find the lowest buckling load.

As can be seen from Table 2, for the stringer stiffened shell XS-1 the buckling load with membrane prebuckling depends strongly on the boundary condition specified. Thus for the SS-3 boundary condition the buckling load is 141.6 lb/in. Stiffening this boundary condition raises the buckling load by 14% for the C-3, 30% for the SS-4 and by 44% for the C-4 boundary condition. Further, the inclusion of the nonlinear prebuckling resulted in buckling loads which are only a few percent lower than the corresponding buckling loads with membrane prebuckling.

Buckling Loads of the Imperfect Shells

Table 2 shows, for the perfect shell, the number of circumferential waves at which bifurcation into an asymmetric buckling mode first occurred varied with the boundary conditions and with the axisymmetric prebuckling analysis used. Hence it became necessary to ascertain for each boundary condition that circumferential wave number which, for a given initial imperfection, would yield the lowest buckling load. This was done by making runs at an axial load level of $\lambda=0.5$ using the same imperfection shapes but varying the number of circumferential waves. As can be seen from Fig. 4 using the SS-3 boundary condition, the maximum amplitude of the asymmetric response has a distinct maximum at $n=11$. Interestingly enough, the potential energy of the system has a minimum at $n=11$ as can be seen from Table 3. Thus for the SS-3 boundary condition the limit point calculations for the imperfect shell were carried out with $n=11$. The values of n used for the other boundary conditions were found in a similar fashion.

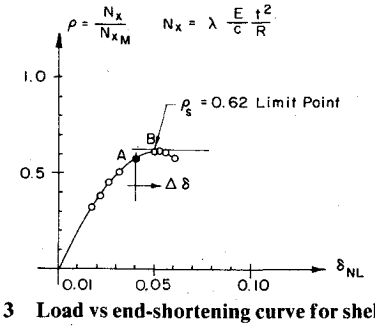

Fig. 3 Load vs end-shortening curve for shell XS-1.

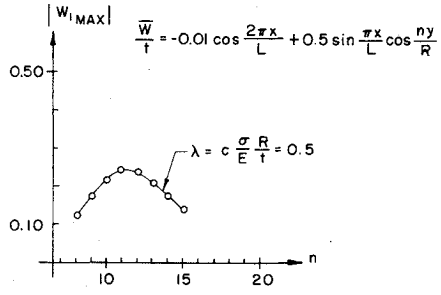

Fig. 4 Variation of deformation with circumferential wave number (SS-3 boundary condition $-N_x = v = W = M_x = 0$).

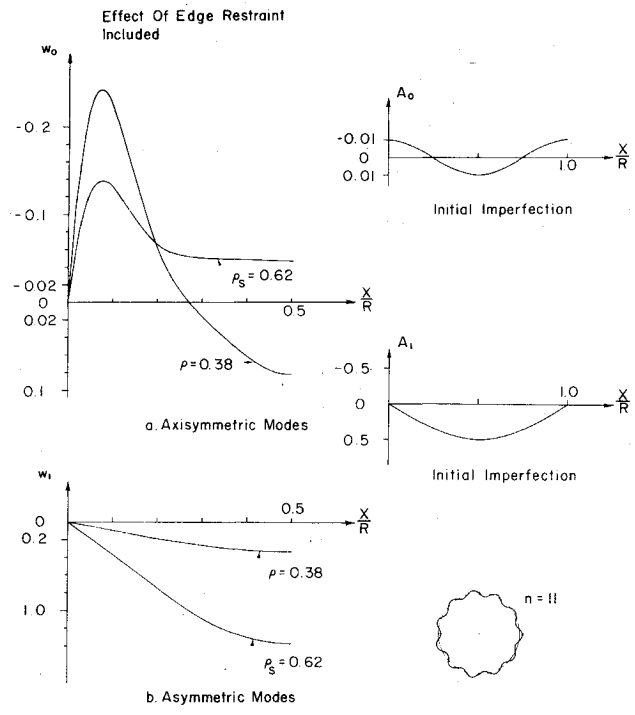

Fig. 5 Calculated radial displacements for SS-3 boundary condition, ($q = 0$).

Figures 5 and 6 show both the axisymmetric and asymmetric components of the prebuckling deformation and of the collapse modes for 2 different sets of boundary conditions. The load levels and the number of circumferential waves used are indicated on the figures. As mentioned earlier, by switching to increments of end-shortening instead of axial load increments it became possible to integrate around the limit point and to obtain solutions for the axial load levels at the respective limit points. In order to reduce the computer time needed for obtaining solutions, the symmetry with respect to the central plane of the shell was used to replace the specified boundary conditions at $\bar{x} = L/R$ by the symmetry condition ($u = N_{xy} = Q_x = w_{,x} = 0$) at $\bar{x} = L/2R$. Then the integration of the boundary value problem [Eq. (19)] had to be carried out only over half the shell length.

As can be seen from Figs. 5 and 6 for the axisymmetric components of the response curves the effect of the edge restraint extends over about 15% of the shell length from each end. Also for the simply supported boundary conditions there is a pronounced overshoot of the axisymmetric radial displacement component w_0 in the boundary regions. Clearly outside these rather wide boundary layers the shape of the axisymmetric responses resembles the full wave cosine initial imperfection modes used as an input in the analysis.

For the simply-supported boundary conditions, the asymmetric components of the radial displacements resemble

Table 3 Variation of potential energy with circumferential wave number at $\rho = 0.32$ ($\lambda = 0.5$)

n	$P = U/2\pi\frac{c^2}{Et^3}\frac{R}{L}$
8	−0.0869161
9	−0.0869619
10	−0.0870035
11	−0.0870247
12	−0.0870173
13	−0.0869891
14	−0.0869544
15	−0.0869224

Table 2 Summary of the buckling load calculations for the stringer stiffened shell XS-1

	SS-3	SS-4	C-3	C-4
N_{x_M}	141.6 (11)	184.5 (15)	161.6 (12)	204.0 (16)
$N_{x_{NL}}$	134.4 (11)	176.7 (12)	160.2 (12)	197.1 (16)
$N_{s_{MM}}$	88.3 (11)	...	...	...
$N_{s_{EXT}}$	87.7 (11)	117.6 (12)	102.5 (11)	125.6 (13)
ρ_s	0.62	0.64	0.63	0.62

Numbers in parentheses are the number of circumferential waves n

N_{x_M} = Perfect shell buckling load using membrane prebuckling analysis [19] (lb/in.)
$N_{x_{NL}}$ = Perfect shell buckling load using nonlinear prebuckling analysis [19] (lb/in.)
$N_{s_{MM}}$ = Imperfect shell buckling load by the multimode analysis [7] (lb/in.)
$N_{s_{EXT}}$ = Imperfect shell buckling load by the extended analysis (lb/in.)
ρ_s = $N_{s_{EXT}}/N_{x_M}$
SS-3 $-N_x = v = W = M_x = 0$
SS-4 $-u = v = W = M_x = 0$
C-3 $-N_x = v = W = W_{,x} = 0$
C-4 $-u = v = W = W_{,x} = 0$

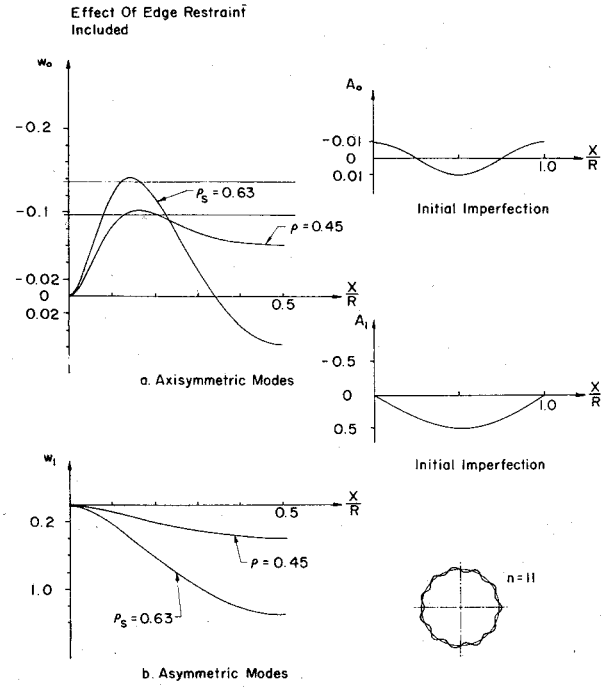

Fig. 6 Calculated radial displacements for C-3 boundary conditions.

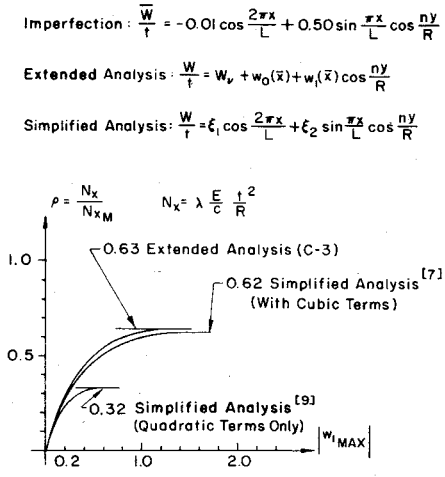

Fig. 7 Comparison between simplified and extended analyses.

closely the half wave sine mode used as an initial imperfection. However, for the clamped boundary conditions at about 15% of the shell length from each end there is an inversion point. The response curves change their curvature there and then approach gradually the condition of zero slope at the shell edges.

Different investigatiors[20,21] have indicated that load eccentricity is an important boundary effect for stringer stiffened shells under axial compression. Our study found[13] that, for imperfect shells, the collapse load was only slightly affected by moderate load eccentricities (of the order of the wall thickness), despite the significant changes produced in the shape of the axisymmetric component of the collapse mode near the shell edges.

Discussion of the Numerical Results

Examining the effect of the following idealized imperfection

$$\bar{W}/t = -0.01\cos 2\pi x/L + 0.50\sin \pi x/L\cos ny/R \qquad (25)$$

consisting of an axisymmetric and an asymmetric mode, it was found that the "multimode analysis" of Ref. 7 and the "extended analysis" with SS-3 boundary condition gave virtually the same buckling load. As can be seen from the results displayed in Table 2, the assumed idealized imperfection resulted in a 38% decrease in the buckling load when compared with the buckling load of the perfect shell for a membrane prebuckling state and the same SS-3 boundary condition. Next the buckling load for the same shell with the same imperfection but with C-3 boundary condition was calculated. This resulted in a 37% decrease in the buckling load when compared with the buckling load of the perfect shell for a membrane prebuckling state and the same C-3 boundary condition. This similarity in the reduction of the buckling load for the two different boundary conditions motivated the decision to take the effect of boundary conditions into account (when they are important) by comparing the buckling load of a imperfect shell to the corresponding buckling load of a perfect shell using in both cases the same boundary conditions. As can be seen from the results tabulated in Table 2, this normalization procedure works well also for the other boundary conditions (SS-4 and C-4) investigated.

These results further suggested that one should be able to account for both the effect of the imperfections and the effect of the appropriate boundary conditions with the help of the following formula

$$N_{s_{C\text{-}4}} = (N_{s_{MM}})\,(N_{x_{C\text{-}4}}/N_{x_{SS\text{-}3}}) \qquad (26)$$

where

$N_{s_{C\text{-}4}}$ = imperfect shell buckling load for C-4 boundary conditions (lb/in.)

$N_{s_{MM}}$ = imperfect shell buckling load by the multimode analysis[7] (lb/in.)

$N_{x_{C\text{-}4}}$ = perfect shell buckling load using membrane prebuckling analysis and C-4 boundary conditions[19] (lb/in.)

$N_{s_{SS\text{-}3}}$ = perfect shell buckling load using membrane prebuckling analysis and SS-3 boundary conditions[19] (lb/in.)

Finally a comparison of the present results with those of the simplified analyses[7,22] revealed a very close agreement, Fig. 7, if in the simplified analysis the half-wave cosine representation for the axisymmetric component and the half-wave sine representation for the asymmetric component are used, and if the buckling loads are normalized as indicated by Eq. (26). The comparison also indicates that the cubic terms in the simplified analyses cannot be neglected.

Conclusions

When calculating the buckling loads of axially compressed, stiffened imperfect cylindrical shells we feel that the close agreement between the rigorous solutions presented in this paper and the properly normalized results of the previously introduced simplified analyses[7,9] justifies the use of the simplified analysis when the axisymmetric components of the initial imperfections point inward over the central portions of the shell.

The investigation into the effect of different boundary conditions in the presence of initial imperfections has lead to a simple normalization procedure, which makes it possible to take into account both the effect of initial imperfections and the effect of the appropriate boundary conditions in the rather simple and inexpensive way given by Eq. (26).

The advantage of this procedure lies in the fact that both the multimode analysis and the perfect shell buckling analysis are relatively inexpensive to run. Thus using the multimode analysis one can investigate the effects of different imperfection models in order to find the lowest buckling load (see Ref. 7 for details of this search procedure). Next, using SRA[19] or any other standard shell of revolution code, one has to calculate the buckling loads of the perfect shell for the

boundary conditions indicated. Finally, using the proposed formula (26), one can take into account both the effect of the initial imperfections and the effect of the appropriate boundary conditions. This procedure eliminates the need for making very expensive computer runs with two-dimensional codes like STAGS.[23]

Also, when using this approach, it is necessary to ascertain that no bifurcation from the present response curve into another mode with $n+\Delta n$ waves will occur before the limit point is reached. As pointed out in Ref. 8 this usually implies that the axisymmetric component of the initial imperfection must point inward over the central portion of the shell.

References

[1]"Thin-Shell Structures Theory, Experiment and Design," edited by Y.C. Fung and E.E. Sechler, Prentice-Hall, Englewood Cliffs, N.J., 1974.

[2]Stein, M., "Some Recent Advances in the Investigation of Shell Buckling," *AIAA Journal,* Vol. 6, Dec. 1968, pp. 2339-2345.

[3]Hutchinson, J.W. and Amazigo, J.C., "Imperfection Sensitivity of Eccentrically Stiffened Cylindrical Shells," *AIAA Journal,* Vol. 5, March 1967, pp. 392-401.

[4]Weller, T., Singer, J. and Batterman, S.C., "Influence of Eccentricity of Loading on Buckling of Stringer-Stiffened Cylindrical Shells," *Thin Shell Structures,* Prentice-Hall, Englewood Cliffs, N.J., 1974.

[5]Hutchinson, J.W., "Axial Buckling of Pressurized Imperfect Cylindrical Shells," *AIAA Journal,* Vol. 3, Aug. 1965, pp. 1461-1466.

[6]Arbocz, J. and Babcock, C.D., "The Effect of General Imperfections on the Buckling of Cylindrical Shells," *Journal of Applied Mechanics,* Vol. 36, March 1969, pp. 28-38.

[7]Arbocz, J. and Babcock, C.D., "Prediction of Buckling Loads Based on Experimentally Measured Initial Imperfections," *Proceedings IUTAM Congress on the Buckling of Structures,* Harvard University, Cambridge, Mass., June 1974.

[8]Arbocz, J. and Sechler, E.E., "On the Buckling of Axially Compressed Imperfect Cylindrical Shells," *Journal of Applied Mechanics,* Vol. 41, Sept. 1974, pp. 737-743.

[9]Arbocz, J., "The Effect of Initial Imperfections on Shell Stability," *Thin Shell Structures,* Prentice-Hall, Englewood Cliffs, N.J., 1974

[10]Geier, B., "Das Beulverhalten Versteifter Zylinderschalen Teil 1. Differential-Gleichungen," *Z. Flugwiss.,* Vol. 14, July 1966, pp. 306-323.

[11]Singer, J., personal communication, 1968.

[12]Thurston, G.A. and Freeland, M.A., "Buckling of Imperfect Cylinders under Axial Compression," NASA, CR-541, July 1966.

[13]Arbocz, J. and Sechler, E.E., "On the Buckling of Axially Compressed Ring and Stringer Stiffened Imperfect Cylindrical Shells," California Institute of Technology, Pasadena, Calif, GALCIT SM 73-10, 1973.

[14]Kempner, J., "Postbuckling Behavior of Axially Compressed Cylindrical Shells," *Journal of Aeronautical Sciences,* Vol. 21, May 1954, p. 329.

[15]Arbocz, J., "On the Problem of Limit Point Calculations," California Institute of Technology, Pasadena, Calif. GALCIT SM 75-7, Nov. 1975.

[16]Arbocz, J. and Sechler, E.E., "On the Buckling of Axially Compressed Imperfect Cylindrical Shells," California Institute of Technology, Pasadena, Calif. GALCIT SM 73-4, April 1973.

[17]Keller, H., "Numerical Methods for Two-Point Boundary Value Problems," Blaisdell Publishing Co., Waltham, Mass., 1968.

[18]Singer, J. and Rosen, A., "Design Criteria for Buckling and Vibration of Imperfect Stiffened Shells, 9th ICAS Congress, Haifa, Israel, Aug. 1974.

[19]Cohen, G.A., "Buckling of Axially Compressed Cylindrical Shells with Ring Stiffened Edges," *AIAA Journal,* Vol. 4, Oct. 1966, pp. 1859-1862.

[20]Block, D.L., "Influence of Prebuckling Deformations, Ring Stiffeners and Load Eccentricity on the Buckling of Stiffened Cylinders," AIAA/ASME 8th Structures, Structural Dynamics and Materials Conference, March 1967, pp. 597-607.

[21]Almroth, B.O. and Bushnell, D., "Computer Analysis of Various Shells of Revolution," *AIAA Journal,* Vol. 6, Oct. 1968, pp. 1848-1856.

[22]Arbocz, J. and Babcock, C.D., "On the Role of Imperfections in Shell Buckling," (Paper presented at the 13th IUTAM Congress in Moscow, Aug. 21-26, 1972). Also GALCIT SM 72-4.

[23]Almroth, B.O., Brogan, F.A. and Zele, F., "Buckling Analysis of General Shell, Vol. II. User's Manual for the STAGS Computer Code," Lockheed Missiles and Space Co., LSMC-D032008, 1970.